nature geoscience

SUPPLEMENTARY INFORMATION

DOI: 10.1038/NGEO526

Supplemental Information for
West et al., Vertical mantle flow associated with a lithospheric drip beneath the Great Basin

Supplementary Methods

Shear wave splitting analysis

A host of evidence suggests that the primary cause of seismic anisotropy in the upper mantle is the lattice-preferred orientation (LPO) of crystallographic axes of elastically anisotropic minerals[1-3]. When olivine is subjected to deformation via dislocation creep as is thought to occur in the upper mantle, the a-axis of the olivine crystals tends to align with the direction of the shear plane under conditions of simple shear and strain >150%[2]. Assuming finite strain is generated over time periods of several My, LPO develops in the upper mantle with the fast axis direction aligned with the direction of flow. Thus, shear-wave splitting is often used as a proxy for mantle flow. While the maximum depth of upper mantle anisotropy is still debated, olivine (the dominant upper mantle mineral) likely deforms in the dislocation creep regime (the deformation regime in which LPO can develop) to depths of 200-400 km[4]. It is also important to note that the relationship between splitting fast direction and mantle flow is only valid in cases of long-term simple shear in dry olivine, as more complex flow patterns, low strain rates, strain accommodated by diffusion creep, and/or the presence of water in the system can alter the relationship between mantle flow and direction of seismic anisotropy[5-7].

When a seismic shear wave passes through an anisotropic material, its energy is split into two orthogonal components which travel at differing velocities. These two components arrive at the measuring instrument separated by a splitting delay time (*dt*). We utilized the method of Silver and Chan[8] and the SplitLab analysis tool set[9] to determine *dt* and the fast polarization direction of the axis of transmission (φ) for each event/station pair. We performed shear-wave splitting analyses by first selecting events with $m_b \geq 5.8$ and epicentral distances between 85 and 130 degrees. All seismograms were bandpass filtered at .02-0.2 Hz, and the time window around the SKS phase was chosen in each case for best and most stable results. Supplementary Figure 1 shows a typical splitting measurement. In this study, we present new shear wave splitting results from 139 broadband seismic stations around the Great Basin region. 106 of these stations are from the USArray Transportable Array (TA), while the other 33 are permanent regional stations. Results from this study include only those measurements exhibiting clear and well-resolved splitting parameters, for a total of 628 new shear wave splitting measurements (Supplementary Table 1) from 148 seismic events (Supplementary Table 2). We note that at many of the long-lived seismic stations, backazimuthal variations in splitting parameters are evident, suggesting the likelihood of complexity in the overall anisotropic character beneath these stations. However, these are generally second-order effects and do not strongly influence the conclusions draw in the work presented here. These new results substantially improve our understanding of anisotropic structure beneath the Great Basin, particularly when combined with existing shear wave splitting measurements in the region [10-27]

DOI: 10.1038/NGEO526

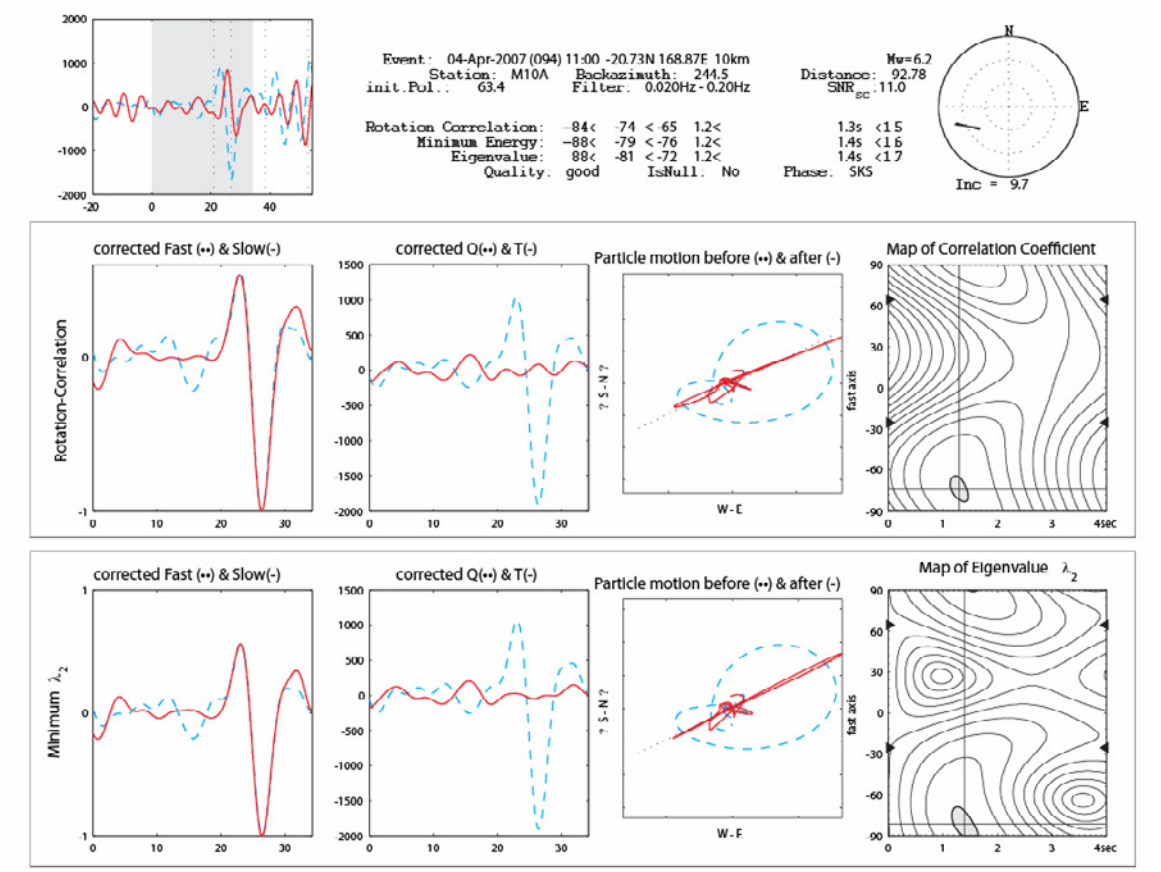

Supplementary Figure 1: Typical shear-wave splitting measurement. Screen shot of a typical shear-wave splitting measurement in SplitLab, showing radial and transverse seismograms of the SKS phase, particle motion plots, and cross-correlation plots.

Seismic tomography and resolution tests

The P-wave seismic tomography model presented in this study, NWUS08-P2, is a significant update from the original model presented in Roth et al.[28] That paper contains supplementary material concerning the data and methodology used in the inversion for P-wave relative delay times. The model presented here includes data for 526 stations and 363 events, with a total of 38,908 raypaths used in the inversion.

The remaining supplementary information presented here focuses on the resolution of the cylinder of increased velocities beneath the central Great Basin (the "Nevada Cylinder" as termed in Roth et al.[28]). The structural resolution tests of the tomographic model are performed using the VanDecar[29] method. In this formulation, model seismic structures are built by assigning slowness values at a series of knots within the model space, with a Gaussian-tapered variation in slowness between peak values. We then utilize these models to predict the relative delay times measured at the receivers using raypaths calculated for each source-receiver pair (assuming a 1D velocity model). In order to approximate the effects of timing and event location errors, we add random noise (+/- $\leq$ 0.3 s) to the delay times predicted from the forward models. We invert the relative delay time dataset simultaneously for the slowness perturbation field, earthquake relocations, and station terms, in order to see if the input structure is well recovered in the inversion. Earthquake relocation parameters absorb contributions to the delay

times from Earth structure outside of the array, while station terms absorb contributions from unknown shallow structure that cannot be resolved by the inversion.

It is necessary to confirm the resolution of the dip and depth extent of near-vertically oriented structures such as the Nevada Cylinder, since we know that these types of structures can be streaked downward into the tomographic model given the steep incidence of raypaths used in our inversion. In order to validate our inferred depth extent of the Nevada Cylinder, we developed a series of structural resolution tests in which we emplaced a 100 km diameter cylindrical increased velocity (+5 %) anomaly. The top of the anomaly is located at the surface (0 km depth), and we tested a series of models where the maximum depth of the cylinder ranged from 200 km to 600 km. Further, we examined a range of models where the dip of the cylinder ranged from vertical to 60º. Examples of these resolution tests are shown in Supplementary Figure 2.

Results of the resolution tests demonstrate that the lateral location of the cylinder is well resolved as previously noted[28]. As expected, the dip of vertical cylinders is not well resolved, but the dip of non-vertical, steeply dipping, cylinders is well resolved. In all tests, the depth extent of the cylinder is well resolved. We note that Roth et al.[28] suggested that the maximum depth of the Nevada Cylinder was ~300 km. The results of these resolution tests demonstrates that the improved coverage from our new inversion demonstrates that the cylinder extends to depths of at least 500 km and perhaps deeper, and that we have correctly imaged the cylinder dip.

It is possible that the Nevada Cylinder may be enhanced by radial anisotropy in the crust and/or mantle. Shallow structures, such as those from radial anisotropy in the crust, will be effectively removed by the station terms computed during the inversion[28], resulting in little to no effect of crustal radial anisotropy in the model. However, drip-induced downwelling flow would be expected to generate radially-oriented mantle anisotropy in the immediate vicinity of the downwelling, depending upon the strain rates and elapsed time since the initiation of flow. Such an orientation of anisotropic fast axis would have the effect of strengthening the P-wave tomographic signature of the cylindrical feature. However, we note that preliminary S-wave tomographic models using the same inversion method presented here[30] also image the cylinder of higher velocities. This indicates that the higher velocities are not due solely to radial anisotropy, which would not significantly influence the S-wave tomographic model, but rather must originate from some combination of thermal and compositional anomalies. This result is further supported by regional surface wave models, which also indicate the presence of the cylinder[31].

DOI: 10.1038/NGEO526

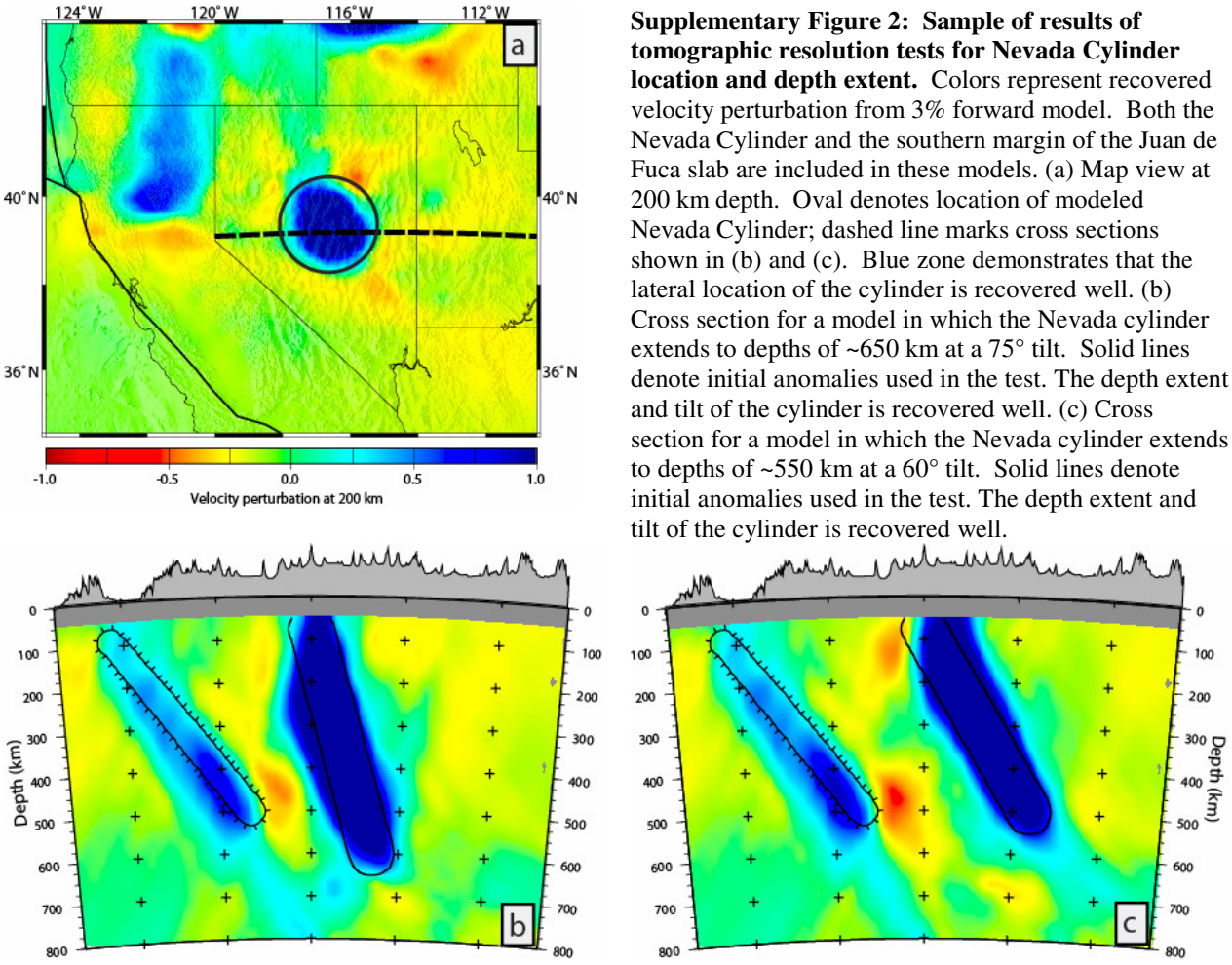

Supplementary Figure 2: Sample of results of tomographic resolution tests for Nevada Cylinder location and depth extent. Colors represent recovered velocity perturbation from 3% forward model. Both the Nevada Cylinder and the southern margin of the Juan de Fuca slab are included in these models. (a) Map view at 200 km depth. Oval denotes location of modeled Nevada Cylinder; dashed line marks cross sections shown in (b) and (c). Blue zone demonstrates that the lateral location of the cylinder is recovered well. (b) Cross section for a model in which the Nevada cylinder extends to depths of ~650 km at a 75° tilt. Solid lines denote initial anomalies used in the test. The depth extent and tilt of the cylinder is recovered well. (c) Cross section for a model in which the Nevada cylinder extends to depths of ~550 km at a 60° tilt. Solid lines denote initial anomalies used in the test. The depth extent and tilt of the cylinder is recovered well.

Geodynamic numerical modeling of lithospheric drips

The numerical experiments are produced using a two-dimensional axisymmetric finite element fluid dynamic code called SSAXC[32,33]. The models include a lithosphere with a flat lower boundary (i.e., no lithospheric root) into which a region of higher-density material has been injected. This denser material is an analog of magmatic flux that has frozen as an eclogite, or has left behind dense mafic cumulates. This material is therefore both denser and warmer than the surrounding lithosphere, and it has a different composition. The denser composition is modeled as a half cosine wave in x with a maximum at the left side of the axisymmetric model box, falling to zero in the positive x direction, and a half cosine wave in z, with a maximum at the bottom of the mantle lithosphere, falling to zero vertically in z. The width of the dense regions is equivalent to 80 km. Temperature is also added to the lithosphere in the same pattern, bringing the region of intrusion closer to the mantle temperature beneath and correspondingly lowering its viscosity. We examine a range of experiments in which we vary the thickness, position, and density contrast of the dense region, as well varying the reference mantle viscosity. The models at several time steps are shown in Supplementary Figures 3-7, and a summary of the experiments is given in Supplementary Table 3. In some numerical experiments the density and temperature is added throughout the thickness of the lithosphere, and in others through only half the thickness of the lithosphere.

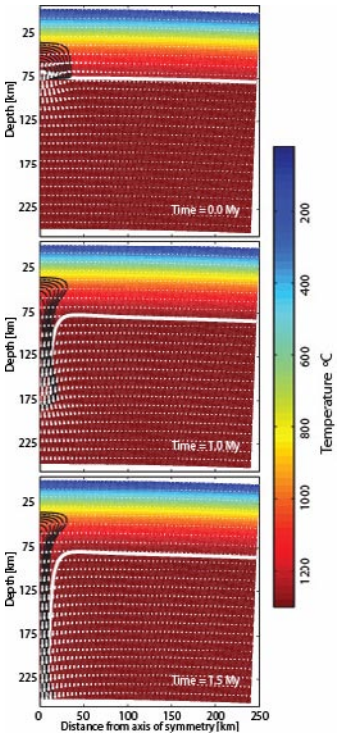

Supplementary Figure 3: Geodynamic model 3540. Model parameters are listed in Supplementary Table 3.

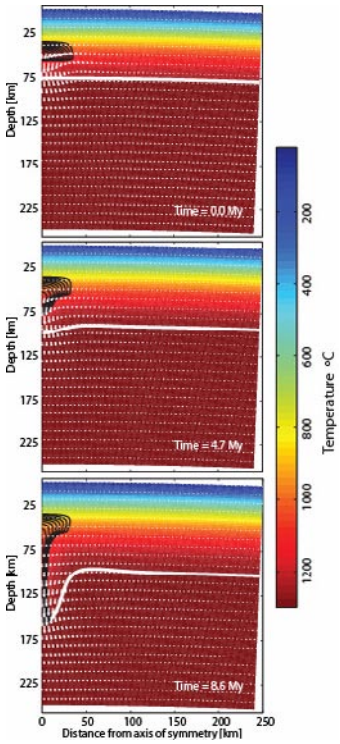

Supplementary Figure 4: Geodynamic model 3540h. Model parameters are listed in Supplementary Table 3.

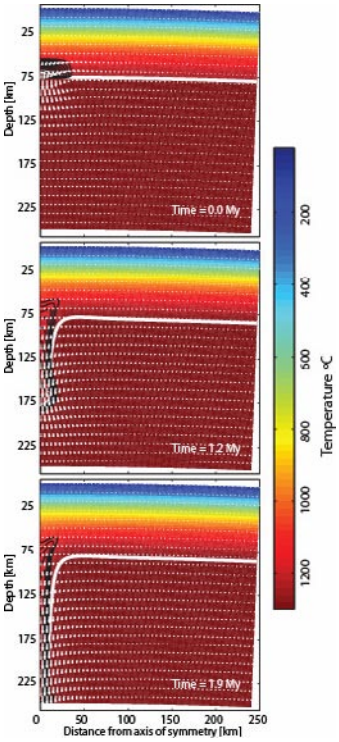

Supplementary Figure 5: Geodynamic model 3540L. Model parameters are listed in Supplementary Table 3.

DOI: 10.1038/NGEO526

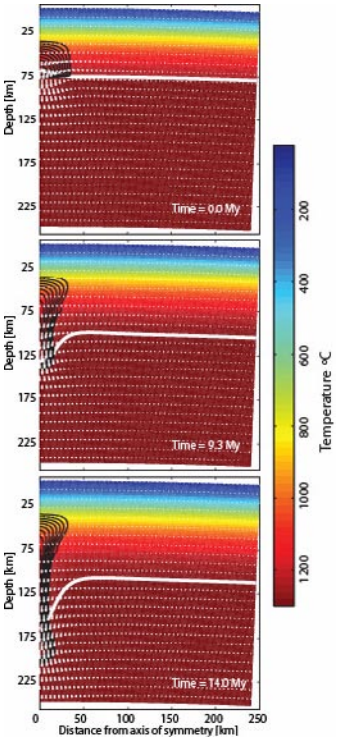

Supplementary Figure 6: Geodynamic model 3540v. Model parameters are listed in Supplementary Table 3.

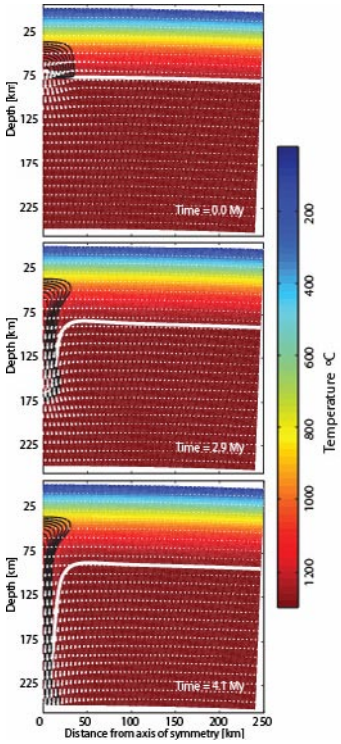

Supplementary Figure 7: Geodynamic model 35401. Model parameters are listed in Supplementary Table 3. This model also shown as Figure 3 in main article.

Supplementary Table 3: Parameters and results for geodynamic models.

Model	**3540**	**3540h**	**3540L**	**3540v**	**35401**
Mantle reference viscosity (Pa s)	10^{19}	10^{19}	10^{19}	10^{20}	10^{19}
Seed density contrast	3%	3%	3%	3%	1%
Seed density thickness (km)	40	20	20	40	40
Seed density depth (km)	75	55	75	75	75
Approximate drip velocity (mm/yr)	110	12	92	9	33

A buoyant crust is included above the mantle lithosphere and its density anomaly[34,35]. The crust differs from the mantle lithosphere in these models only in its buoyancy. The modeled crust and mantle lithospheric material both possess the same temperature dependence of viscosity and the same thermal diffusivity as the underlying convecting mantle, though the cooler temperatures in the lithosphere and crust produce higher viscosities.

The model box consists of a 100 by 100 grid of nodes that correspond to a domain of 250 by 250 km. The left-hand side of the model box is an axis of symmetry. The bottom and right sides have flow-through boundary conditions, and the top is a free-slip boundary with its temperature set to the nondimensional equivalent of 20°C. The code solves nondimensional equations for flow as given in[36] comprises an equation of motion,

$$\nabla \bullet (\eta \dot{\varepsilon}) - \nabla P = (RaT - Ra_c \Gamma)\hat{z}\,, \tag{1}$$

a statement of incompressibility,

$$\nabla \bullet v = 0\,, \tag{2}$$

an advection-diffusion equation for temperature,

$$\frac{\partial T}{\partial t} + (v \bullet \nabla)T = \nabla^2 T\,, \tag{3}$$

and an advection equation for composition,

$$\frac{\partial \Gamma}{\partial t} + (v \bullet \nabla)\Gamma = 0, \tag{4}$$

depending upon viscosity (η), the deviatoric strain rate tensor ($\dot{\varepsilon}$), dynamic pressure (P), thermal and compositional Rayleigh numbers (Ra and Ra_c, given below), composition (Γ), velocity (v), temperature (T), time (t), and the unit vector in the direction of gravity ($\hat{z}$).

Both temperature and composition contribute to buoyancy. Thermal buoyancy is determined by the Raleigh number, containing terms for density (ρ), gravity (g), thermal expansivity (α), temperature range across the model box (ΔT), height of the model box (h), reference viscosity (η_o), and thermal diffusivity (κ):

$$Ra = \frac{\rho g \alpha \Delta T h^3}{\eta_o \kappa} = 2 \times 10^6\,. \tag{5}$$

Both the negative buoyancy of the dense lower lithosphere and the positive buoyancy of the crust are measured by the compositional Rayleigh number,

$$Ra_c = \frac{\Delta \rho g h^3}{\eta_o \kappa} = Ra\left[\frac{\Delta \rho}{\rho \alpha \Delta T}\right] \tag{6}$$

in which $\Delta\rho$ is the difference between the densities of the lower lithospheric composition and the adjoining asthenosphere. The dense material in the lithosphere is set to a 1%-3% density increase over adjacent mantle lithosphere, and its maximum temperature addition is 10% above the

DOI: 10.1038/NGEO526

ambient asthenospheric temperature, consistent with heats of fusion. The buoyant crust is set to a 12% density decrease when compared to reference mantle density.

Viscosity is calculated in most experiments using the following Newtonian law:

$$\eta_{Newtonian.} = \eta_o \exp\left(\frac{E+Vz}{T+T_o} - \frac{E+Vz_o}{1+T_o}\right), \quad (7)$$

where η_o, z_o, and T_o are reference values for viscosity, depth, and temperature, respectively; E is the activation energy, and V is the reference volume (Supplementary Table 4). The importance of the temperature dependence of viscosity is investigated by using values for the activation energy E equivalent to either 250 or 500 kJ/mol. The reference mantle temperature T_o is 1300°C.

A starting condition for each numerical experiment was created by using a complementary error function cooling law to make a cooled lithosphere of the desired depth, employing the temperature at the surface (T_S), the temperature of the convecting mantle (T_M), thermal diffusivity (κ), and the time period of thermal diffusion (τ)[37]:

$$T(z) = (T_S - T_M)erfc\left[\frac{z}{2(\kappa\tau)^{0.5}}\right] + T_M \quad (8)$$

to create a lithosphere of 75 km thickness. There is no imposed initial mantle flow field.

Any melt produced by dry adiabatic melting in convection currents associated with the gravitational instability is calculated with a post-processor routine using the parameters listed in Supplementary Table 4. This postprocessor routine uses the mantle flow fields to calculate the volume of asthenospheric material moving above its solidus during each time step of the numerical calculations. Melt is produced at a rate of 0.1% per degree rise above the solidus, which is fitted to experimental data on the continental fertile peridotite KLB-1[38,39]. The models presented here do not produce melt.

The surface topography resulting from stresses imposed on the lithosphere by the density anomaly and its subsequent gravitational instability are calculated from differential stress values at the surface produced by the numerical calculations. The magnitude of topography calculated from deviatoric stress output from numerical models is highly dependent upon the scaling parameters used. Here we use the same scaling parameters used for the numerical experiments themselves. If other scaling rules are used, the magnitude of the topographic expression will change, but not its sense. Only minimal topographic deviation is produced by this minimally dense downwelling material, as covered in detail in an earlier paper by Elkins-Tanton[40].

Supplementary Table 4: Parameters common to numerical models of dripping lithosphere.

Parameter	Symbol	Value
Height and width of model box	h	250 km
Number of nodes in each dimension of the model box		100
Reference mantle density	ρ	3,300 kg/m^3
Crustal density		2,900 kg/m^3

Reference viscosity	η_0	10^{19}-10^{20} Pa s
Thermal expansivity	α	3×10^{-5} /°
Thermal diffusivity	κ	1×10^{-6} m^2/s
Rayleigh number	Ra	2×10^{6}
Density contrast between altered lower lithosphere and asthenosphere	$\Delta\rho$	1%-3%
Compositional Rayleigh number	Ra_c	5×10^{5}
Mantle potential temperature	T_p	1,300°C
Heat capacity of silicates	C_P	1256.1 J/°kg
Heat of fusion of silicates	H_f	418,700 J/kg

Estimates of the volume of the Great Basin Drip

Tomographic images of the Great Basin Drip show a structure which can be approximated as a near-vertical cylinder of diameter ~100 km, and extending from the base of the lithosphere at a depth of ~75 km to a depth of at least 500 km and perhaps deeper. The near-surface structure is not well resolved using our methods, and below 500 km depth the drip appears to merge with a larger high-velocity region. We image a well-resolved NE dip to the cylinder from which we deduce that the possible length of the drip may be as much as 500 km. Our range of geodynamic models of the drip in many cases show effective drip radii smaller than 50 km, we therefore evaluate a range of possible drip radii ranging from 25 to 50 km and a maximum sublithospheric drip length of 500 km. We used these values to make a very rough estimate of cylinder volume, which ranges from 1 to 4 million km^3.

In our geodynamic models, the source of the drip draws material from a wide volume, which can be approximated as a disk near the base of the lithosphere incorporating both lithospheric and asthenospheric material. Assuming that the radius of the source disk is ~10 times that of the drip implies that the drip has drawn material from a disk ~250-500 km in radius. Given the drip volume range calculated above, the drip would draw material from a source disk thickness of ~5 km over the area of the source disk; smaller-diameter source disks would be thicker. The tradeoff between source disk radius, source disk thickness, and drip radius is shown in Supplementary Figure 8. We note, however, that these estimates are only meant to provide intuition regarding the regional effects of the volume drawn into the drip, since a much larger range of factors can influence regional lithospheric and asthenospheric modification.

DOI: 10.1038/NGEO526

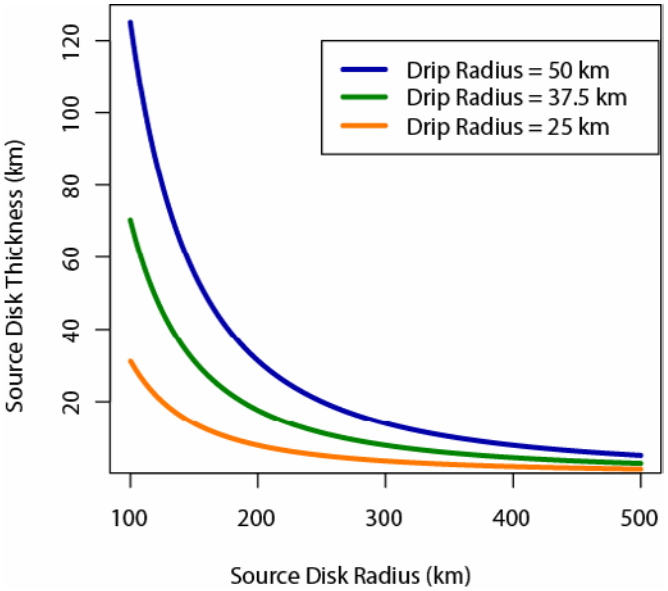

Supplementary Figure 8: Relationship between drip radius, source disk size, and source disk thickness. Three curves are shown, corresponding to drip radii of 25, 37.5, and 50 km. The curves show thickness of a source disk feeding the drip, related to disk radius.

Constraints on the mantle flow direction beneath the western U.S.

In the absence of background mantle flow, the Great Basin Drip would be expected to descend vertically into the mantle. However, resolution tests show that the dip of the high-velocity region is not due to smearing effects, and the dip angle is well resolved. Given the NE dip of the Great Basin Drip, we therefore infer that the mantle flow direction relative to the North American plate is ~NE, or opposite the direction of North American plate motion in the hotspot reference frame[41]. However, because it is not possible to estimate drip descent velocity given the wide range of parameters responsible for the downwelling, we are unable to estimate a more detailed mantle flow field at this point in time.

References:

1 Silver, P. G. Seismic anisotropy beneath the continents: Probing the depths of geology. *Annu. Rev. Earth Planet. Sci.* **24**, 385-432 (1996).

2 Savage, M. K. Seismic anisotropy and mantle deformation: What have we learned from shear wave splitting? *Rev. Geophys.* **37**, 65-106 (1999).

3 Fouch, M. J. & Rondenay, S. Seismic anisotropy beneath stable continental interiors. *Phys. Earth Planet. Inter.* **158**, 292-320, doi:10.1016/j.pepi.2006.03.024 (2006).

4 Karato, S. & Wu, P. Rheology of the upper mantle - a synthesis. *Science* **260**, 771-778 (1993).

5 Jung, H. & Karato, S. Water-induced fabric transitions in olivine. *Science* **293**, 1460-1463 (2001).

6 Kaminski, E. & Ribe, N. M. Timescales for the evolution of seismic anisotropy in mantle flow. *Geochem. Geophys. Geosyst.* **3**, doi:1051 10.1029/2001gc000222 (2002).

7 Lassak, T. M., Fouch, M. J., Hall, C. E. & Kaminski, E. Seismic characterization of mantle flow in subduction systems: Can we resolve a hydrated mantle wedge? *Earth Planet. Sci. Lett.* **243**, 632-649, doi:10.1016/j.epsl.2006.01.022 (2006).

8 Silver, P. G. & Chan, W. W. Shear-wave splitting and subcontinental mantle deformation. *J. Geophys. Res.* **96**, 16429-16454 (1991).

9 Wüstefeld, A., Bokelmann, G., Zaroli, C. & Barruol, G. SplitLab: A shear-wave splitting environment in Matlab. *Comput. Geosci.* **34**, 515-528, doi:10.1016/j.cageo.2007.08.002 (2008).

10 *Arizona State University Upper Mantle Anisotropy Database*, <http://geophysics.asu.edu/anisotropy/upper> (2008).

11 Davis, P. M. Azimuthal variation in seismic anisotropy of the southern California uppermost mantle. *J. Geophys. Res.* **108**, doi:2052 10.1029/2001jb000637 (2003).

12 Gök, R. *et al.* Shear wave splitting and mantle flow beneath LA RISTRA. *Geophys. Res. Lett.* **30**, doi:1614 10.1029/2002gl016616 (2003).

13 Hartog, R. & Schwartz, S. Y. Subduction-induced strain in the upper mantle east of the Mendocino triple junction, California. *J. Geophys. Res.* **105**, 7909-7930 (2000).

14 Kubo, A. & Hiramatsu, Y. On presence of seismic anisotropy in the asthenosphere beneath continents and its dependence on plate velocity: Significance of reference frame selection. *Pure Appl. Geophys.*, 281-303 (1998).

15 Özalaybey, S. & Savage, M. K. Shear-wave splitting beneath western United States in relation to plate tectonics. *J. Geophys. Res.* **100**, 18135-18149 (1995).

16 Polet, J. & Kanamori, H. Anisotropy beneath California: shear wave splitting measurements using a dense broadband array. *Geophys. J. Int.* **149**, 313-327 (2002).

17 Savage, M. K. & Sheehan, A. F. Seismic anisotropy and mantle flow from the Great Basin to the Great Plains, western United States. *J. Geophys. Res.* **105**, 13715-13734 (2000).

18 Savage, M. K., Sheehan, A. F. & Lerner-Lam, A. Shear wave splitting across the Rocky Mountain Front. *Geophys. Res. Lett.* **23**, 2267-2270 (1996).

19 Savage, M. K. & Silver, P. G. Mantle deformation and tectonics - constraints from seismic anisotropy in the western United States. *Phys. Earth Planet. Inter.* **78**, 207-227 (1993).

20 Savage, M. K., Silver, P. G. & Meyer, R. P. Observations of teleseismic shear-wave splitting in the Basin and Range from portable and permanent stations. *Geophys. Res. Lett.* **17**, 21-24 (1990).

21 Schutt, D., Humphreys, E. D. & Dueker, K. Anisotropy of the Yellowstone hot spot wake, eastern Snake River Plain, Idaho. *Pure Appl. Geophys.* **151**, 443-462 (1998).

22 Sheehan, A. F., Jones, C. H., Savage, M. K., Özalaybey, S. & Schneider, J. M. Contrasting lithospheric structure between the Colorado Plateau and Great Basin: Initial results from Colorado Plateau - Great Basin PASSCAL experiment. *Geophys. Res. Lett.* **24**, 2609-2612 (1997).

23 Vinnik, L. P., Makeyeva, L. I., Milev, A. & Usenko, A. Y. Global patterns of azimuthal anisotropy and deformations in the continental mantle. *Geophys. J. Int.* **111**, 433-447 (1992).

24 Waite, G. P., Schutt, D. L. & Smith, R. B. Models of lithosphere and asthenosphere anisotropic structure of the Yellowstone hot spot from shear wave splitting. *J. Geophys. Res.* **110**, doi:B11304 10.1029/2004jb003501 (2005).

25 Walker, K. T., Bokelmann, G. H. R. & Klemperer, S. L. Shear-wave splitting beneath the Snake River Plain suggests a mantle upwelling beneath eastern Nevada, USA. *Earth Planet. Sci. Lett.* **222**, 529-542, doi:10.1016/j.epsl.2004.03.024 (2004).

26 Wang, X. L. *et al.* Shear-wave splitting and mantle flow beneath the Colorado Plateau and its boundary with the Great Basin. *Bull. Seismol. Soc. Am.* **98**, 2526-2532, doi:10.1785/0120080107 (2008).

27 Xue, M. & Allen, R. M. Origin of the Newberry Hotspot Track: Evidence from shear-wave splitting. *Earth Planet. Sci. Lett.* **244**, 315-322, doi:10.1016/j.epsl.2006.01.066 (2006).

28 Roth, J. B., Fouch, M. J., James, D. E. & Carlson, R. W. Three-dimensional seismic velocity structure of the northwestern United States. *Geophys. Res. Lett.* **35**, 6, doi:L15304 10.1029/2008gl034669 (2008).

29 VanDecar, J. C. *Upper-mantle structure of the Cascadia subduction zone from non-linear teleseismic traveltime inversion* Ph.D. thesis, University of Washington, (1991).

30 Fouch, M. J., Roth, J. B., James, D. E. & Carlson, R. W. Seismic structure and tectonic evolution of the northwestern United States. *in prep.* (2008).

31 Yang, Y. J. & Ritzwoller, M. H. Teleseismic surface wave tomography in the western US using the Transportable Array component of USArray. *Geophys. Res. Lett.* **35**, doi:L04308 10.1029/2007gl032278 (2008).

32 King, S. D., Raefsky, A. & Hager, B. H. CONMAN - Vectorizing a finite-element code for incompressible 2-dimensional convection in the Earth's Mantle. *Phys. Earth Planet. Inter.* **59**, 195-207 (1990).

33 Elkins-Tanton, L. T. Continental magmatism caused by lithospheric delamination. in *Plates, Plumes, and Paradigms* Special Paper **388** (ed G.R. Foulger, Natland, J.H., Presnall, D.C., and Anderson, D.L.) 449–461 (Geological Society of America, Boulder, CO, 2005).

34 Neil, E. A. & Houseman, G. A. Rayleigh-Taylor instability of the upper mantle and its role in intraplate orogeny. *Geophys. J. Int.* **138**, 89-107 (1999).

35 Hoogenboom, T. & Houseman, G. A. Rayleigh-Taylor instability as a mechanism for corona formation on Venus. *Icarus* **180**, 292-307, doi:10.1016/j.icarus.2005.11.001 (2006).

36 van Keken, P. E. *et al.* A comparison of methods for the modeling of thermochemical convection. *J. Geophys. Res.* **102**, 22477-22495 (1997).

37 Turcotte, D. L. & Schubert, G. *Geodynamics*. 2nd edn, (Cambridge University Press, Cambridge, 2002).

38 Herzberg, C., Raterron, P. & Zhang, J. New experimental observations on the anhydrous solidus for peridotite KLB-1. *Geochem. Geophys. Geosyst.* **1**, doi:10.1029/2000GC000089 (2000).

39 Takahashi, E., Shimazaki, T., Tsuzaki, Y. & Yoshida, H. Melting study of a peridotite KLB-1 to 6.5 GPa, and the origin of basaltic magmas. *Philos. Trans. R. Soc. London Ser. A* **342**, 105-120 (1993).

40 Elkins-Tanton, L. T. Continental magmatism, volatile recycling, and a heterogeneous mantle caused by lithospheric gravitational instabilities. *J. Geophys. Res.* **112**, doi:B03405 10.1029/2005jb004072 (2007).

41 Gripp, A. E. & Gordon, R. G. Young tracks of hotspots and current plate velocities. *Geophys. J. Int.* **150**, 321-361 (2002).

Supplementary Table 1: New shear wave splitting measurements presented in this study.

Phase, seismic phase; dt, splitting time, phi, fast polarization direction,

Event ID, events listed in Supplementary Table 2.

Station	Latitude(∫N)	Longitude(∫E)	Phase	dt(sec)	dt_error(sec)	phi (degrees)	phi_error(degrees)	Event ID
BMN	40.43	-117.22	SKS	.3	.1	-67	8	20030513a
BMN	40.43	-117.22	SKS	.4	.1	-67	5	19950629a
BMN	40.43	-117.22	SKS	.5	.1	-84	8	20020630a
BMN	40.43	-117.22	SKS	.6	.1	-74	7	19970904a
BMN	40.43	-117.22	SKS	.6	.1	-81	7	20000614a
BMN	40.43	-117.22	SKS	.6	.2	-85	8	19961105a
BMN	40.43	-117.22	SKS	.6	.2	77	8	19990913a
BMN	40.43	-117.22	SKS	.7	0	-85	6	19970525a
BMN	40.43	-117.22	SKS	.7	.1	-88	7	20030930b
BMN	40.43	-117.22	SKS	.8	.1	-86	5	20000815a
BMN	40.43	-117.22	SKS	.8	.2	-87	7	20030504a
BMN	40.43	-117.22	SKS	.9	.2	67	9	19950505a
BMN	40.43	-117.22	SKS	.9	.2	88	9	19990801a
BMN	40.43	-117.22	SKS	1.0	.1	82	7	19970503a
BMN	40.43	-117.22	SKS	1.1	.1	89	6	20000610a
BMN	40.43	-117.22	SKS	1.3	.3	78	9	20000621a
BMN	40.43	-117.22	SKS	1.5	.3	69	9	20041015a
BMN	40.43	-117.22	SKS	1.8	.1	-76	3	20010614a
BMN	40.43	-117.22	SKS	2.0	.1	-82	5	20040722a

DOI: 10.1038/NGEO526

BMN	40.43	-117.22	SKS	2.1	.4	89	6	20020610a
CCPE5	36.06	-117.79	SKS	1.6	.2	-74	6	19991101a
CCPS2	36.06	-117.82	SKS	1.5	.1	77	11	19991101a
CCPS5	36.05	-117.83	SKS	1.5	.1	84	7	19991101a
DAN	34.63	-115.38	SKS	1.5	.2	-77	5	20011012a
EDW2	34.88	-117.99	SKS	1.3	.1	70	9	20070130a
EDW2	34.88	-117.99	SKS	1.4	.1	87	8	20041015a
EDW2	34.88	-117.99	SKS	1.4	.2	68	13	20040722a
EDW2	34.88	-117.99	SKS	1.5	.2	39	6	20050205c
EDW2	34.88	-117.99	SKS	1.6	.1	-79	6	20051121a
EDW2	34.88	-117.99	SKS	1.8	.1	-82	6	20051015a
EDW2	34.88	-117.99	SKS	1.9	.1	89	6	20070906a
ELFS	40.61	-120.73	SKS	1.1	.1	90	7	20070718a
ELFS	40.61	-120.73	SKS	1.5	.1	64	8	20070726a
ELFS	40.61	-120.73	SKS	2.2	.2	-79	4	20070820a
ELK	40.74	-115.23	SKS	.3	.2	-43	9	20060218a
ELK	40.74	-115.23	SKS	.5	.2	-75	8	20070404c
ELK	40.74	-115.23	SKS	.6	.1	-69	6	20030513a
ELK	40.74	-115.23	SKS	.6	.1	-83	7	20010603a
ELK	40.74	-115.23	SKS	.6	.2	-87	7	20050723a
ELK	40.74	-115.23	SKS	.7	.1	-36	5	19950629a
ELK	40.74	-115.23	SKS	.7	.1	77	9	20041015a
ELK	40.74	-115.23	SKS	.8	.2	-59	9	19950703a
ELK	40.74	-115.23	SKS	.9	.1	-55	4	19960827a
ELK	40.74	-115.23	SKS	.9	.1	-74	6	20000614a

ELK	40.74	-115.23	SKS	.9	.1	-82	7	20030504a
ELK	40.74	-115.23	SKS	.9	.2	-73	8	20030427a
ELK	40.74	-115.23	SKS	.9	.2	-84	6	19990719a
ELK	40.74	-115.23	SKS	.9	.2	-84	6	20050711a
ELK	40.74	-115.23	SKS	1.0	.1	-50	4	19950117a
ELK	40.74	-115.23	SKS	1.0	.1	-75	5	20000815a
ELK	40.74	-115.23	SKS	1.0	.2	-73	6	20020630a
ELK	40.74	-115.23	SKS	1.0	.2	-84	5	20020819a
ELK	40.74	-115.23	SKS	1.0	.2	-84	7	20021004a
ELK	40.74	-115.23	SKS	1.1	.1	-57	1	19950117a
ELK	40.74	-115.23	SKS	1.3	.3	-78	9	20021210a
ELK	40.74	-115.23	SKS	1.4	.2	-81	9	20060226a
ELK	40.74	-115.23	SKS	2.1	.2	74	8	19991126a
GRA	36.99	-117.37	SKS	1.4	.1	90	7	20041015a
GRA	36.99	-117.37	SKS	1.5	.2	-89	12	20070420a
GRA	36.99	-117.37	SKS	1.6	.1	76	5	20060516a
GRA	36.99	-117.37	SKS	2.3	.1	-77	6	20070403c
GSC	35.30	-116.81	SKS	.8	.2	80	13	19970813a
GSC	35.30	-116.81	SKS	1.2	.2	-71	6	20060516a
GSC	35.30	-116.81	SKS	1.5	.1	-58	3	19990420a
GSC	35.30	-116.81	SKS	1.7	.2	-83	4	19950823a
HATC	40.81	-121.46	SKS	1.2	.2	51	8	20070726a
HEC	34.82	-116.33	SKS	1.2	.1	69	6	20060516a
HEC	34.82	-116.33	SKS	1.2	.2	88	10	20050210a
HEC	34.82	-116.33	SKS	1.4	.2	-87	2	20070928f

DOI: 10.1038/NGEO526

HUMO	42.60	-122.96	SKS	1.6	.2	28	8	20070926a
HUMO	42.60	-122.96	SKS	1.8	0	62	3	20070726a
HUMO	42.60	-122.96	SKS	2.2	.2	53	6	20070731c
HUMO	42.60	-122.96	SKS	2.3	.2	47	6	20070421a
HUMO	42.60	-122.96	SKS	2.4	.1	60	4	20070820b
HUMO	42.60	-122.96	SKS	2.4	.2	59	4	20070614b
HUMO	42.60	-122.96	SKS	2.6	.2	62	8	20070317a
HUMO	42.60	-122.96	SKS	2.7	.1	65	5	20070529b
HUMO	42.60	-122.96	SKS	2.8	.1	66	4	20070722a
J02A	43.36	-123.57	SKS	1.6	.1	60	6	20070117a
J02A	43.36	-123.57	SKS	1.8	.1	77	4	20070726a
J03A	43.37	-122.96	SKS	1.9	.1	70	4	20070726a
J03A	43.37	-122.96	SKS	1.9	.1	51	6	20070722a
J03A	43.37	-122.96	SKS	1.9	.2	46	7	20070421a
J04A	43.24	-122.11	SKS	2.1	.1	86	2	20070726a
J05A	43.28	-121.24	SKS	1.9	.2	86	5	20070726a
J06A	43.25	-120.15	SKS	1.8	.2	-82	8	20070906a
J07A	43.37	-119.31	SKS	1.2	.1	-83	10	20070805a
J07A	43.37	-119.31	SKS	1.9	.2	-52	8	20070727a
J07A	43.37	-119.31	SKS	2.2	.1	87	4	20070726a
J08A	43.35	-118.47	SKS	2.2	.2	77	6	20070718a
J08A	43.35	-118.47	SKS	2.2	.2	72	8	20070906a
J08A	43.35	-118.47	SKS	2.3	.1	77	4	20070131a
J08A	43.35	-118.47	SKS	2.6	.1	71	4	20070517a
J09A	43.34	-117.75	SKS	1.8	0	72	4	20070726a

J09A	43.34	-117.75	SKS	2.0	.1	69	7	20070820a
J09A	43.34	-117.75	SKS	2.1	.1	69	6	20070722b
J09A	43.34	-117.75	SKS	2.4	.1	80	2	20070722a
J09A	43.34	-117.75	SKS	2.5	.1	68	5	20070117a
J09A	43.34	-117.75	SKS	2.6	.2	79	6	20070820b
J10A	43.42	-116.77	SKS	1.7	.1	63	4	20070726a
J10A	43.42	-116.77	SKS	1.8	.2	-87	6	20070718a
J10A	43.42	-116.77	SKS	2.3	.2	-86	6	20070317a
J10A	43.42	-116.77	SKS	2.3	0	82	4	20070906a
J11A	43.41	-115.83	SKS	2.2	.2	-54	9	20070906a
J12A	43.25	-115.10	SKS	1.5	.2	-78	9	20070805a
J12A	43.25	-115.10	SKS	1.6	0	-89	6	20070906a
JCC	40.81	-124.03	SKS	1.4	.2	70	8	20070816a
K01A	42.80	-124.47	SKS	1.9	.1	77	6	20070726a
K02A	42.76	-123.49	SKS	1.8	.1	61	5	20070614b
K02A	42.76	-123.49	SKS	1.9	.2	-83	5	20070726a
K02A	42.76	-123.49	SKS	3.0	.1	34	4	20070421a
K05A	42.72	-120.89	SKS	1.8	.1	85	4	20070726a
K05A	42.72	-120.89	SKS	2.2	.2	73	8	20070317a
K05A	42.72	-120.89	SKS	2.7	.1	80	4	20070906a
K05A	42.72	-120.89	SKS	2.9	.2	76	2	20070529a
K06A	42.79	-120.25	SKS	1.6	.1	-78	7	20070516a
K06A	42.79	-120.25	SKS	2.1	.1	85	4	20070726a
K06A	42.79	-120.25	SKS	2.4	.1	-83	4	20070820a
K06A	42.79	-120.25	SKS	2.5	.1	-79	6	20070906a

DOI: 10.1038/NGEO526

K07A	42.69	-119.25	SKS	1.8	.1	85	3	20070928b
K07A	42.69	-119.25	SKS	1.9	.2	87	5	20070726a
K07A	42.69	-119.25	SKS	2.0	.1	-88	4	20070517a
K07A	42.69	-119.25	SKS	2.1	.1	-88	6	20070906a
K07A	42.69	-119.25	SKS	2.3	.1	88	4	20070529b
K07A	42.69	-119.25	SKS	2.3	.2	79	7	20070820a
K07A	42.69	-119.25	SKS	2.4	.2	81	6	20070131a
K07A	42.69	-119.24	SKS	.5	.1	-55	7	20060815a
K07A	42.69	-119.24	SKS	.6	.2	-64	7	20060807a
K07A	42.69	-119.24	SKS	1.0	.2	-65	6	20070403c
K07A	42.69	-119.24	SKS	1.0	.2	49	8	20070722a
K07A	42.69	-119.24	SKS	1.4	.1	-87	8	20060811a
K07A	42.69	-119.24	SKS	1.6	.1	-88	5	20060917a
K07A	42.69	-119.24	SKS	1.9	.3	77	8	20060916a
K07A	42.69	-119.24	SKS	2.1	.3	89	7	20070516a
K07A	42.69	-119.24	SKS	2.2	.2	82	7	20070517a
K07A	42.69	-119.24	SKS	2.4	.1	69	6	20060903a
K07A	42.69	-119.24	SKS	2.4	.2	89	3	20070529b
K08A	42.73	-118.48	SKS	.9	.2	-57	4	20061003a
K08A	42.73	-118.48	SKS	1.0	.2	-61	8	20070404c
K08A	42.73	-118.48	SKS	1.0	.2	-66	4	20060807a
K08A	42.73	-118.48	SKS	1.0	.2	-67	5	20060807a
K08A	42.73	-118.48	SKS	1.7	.1	-87	4	20060917a
K08A	42.73	-118.48	SKS	1.7	.1	-87	4	20060917a
K08A	42.73	-118.48	SKS	1.7	.2	-51	5	20070403c

K08A	42.73	-118.48	SKS	1.7	.3	74	9	20060916a
K08A	42.73	-118.48	SKS	1.9	.2	88	7	20070517a
K08A	42.73	-118.49	SKS	1.7	.1	-86	5	20070928b
K08A	42.73	-118.49	SKS	1.8	.2	-84	6	20070403c
K08A	42.73	-118.49	SKS	2.0	.1	-85	6	20070517a
K08A	42.73	-118.49	SKS	2.1	.2	47	10	20070529b
K08A	42.73	-118.49	SKS	2.2	.1	78	6	20070726a
K08A	42.73	-118.49	SKS	2.4	.1	90	4	20070906a
K09A	42.69	-117.72	SKS	1.2	.1	-83	4	20060807a
K09A	42.69	-117.72	SKS	1.3	.2	89	4	20070516a
K09A	42.69	-117.72	SKS	1.5	.3	84	8	20060917a
K09A	42.69	-117.72	SKS	2.0	.4	74	9	20070529b
K09A	42.69	-117.72	SKS	2.3	.2	67	6	20060811a
K09A	42.70	-117.73	SKS	1.4	.2	-80	10	20070727a
K09A	42.70	-117.73	SKS	1.7	.1	44	8	20070820a
K09A	42.70	-117.73	SKS	1.8	.2	75	8	20070529b
K09A	42.70	-117.73	SKS	2.0	.1	88	4	20070928b
K09A	42.70	-117.73	SKS	2.4	.1	89	4	20070131a
K09A	42.70	-117.73	SKS	2.5	.2	75	6	20070517a
K09A	42.70	-117.73	SKS	2.8	.2	48	6	20070420a
K10A	42.77	-116.87	SKS	1.2	.1	-57	5	20070404c
K10A	42.77	-116.87	SKS	1.4	.3	-54	6	20070403a
K10A	42.77	-116.87	SKS	1.8	.2	-77	8	20070718a
K10A	42.77	-116.87	SKS	2.1	.2	-81	6	20070517a
K10A	42.77	-116.87	SKS	1.4	.1	-39	4	20070404c

DOI: 10.1038/NGEO526

K10A	42.77	-116.87	SKS	1.5	.2	-51	10	20070927a
K10A	42.77	-116.87	SKS	1.6	.1	-82	5	20070718a
K10A	42.77	-116.87	SKS	1.9	.2	-89	6	20070517a
K10A	42.77	-116.87	SKS	2.0	.1	-86	6	20070906a
K11A	42.77	-116.03	SKS	1.4	.1	-40	6	20070927a
K11A	42.77	-116.03	SKS	1.5	.1	-73	6	20070517a
K11A	42.77	-116.03	SKS	1.5	.1	-62	9	20070404c
K11A	42.77	-116.03	SKS	1.6	0	-71	4	20070727a
K11A	42.77	-116.03	SKS	1.8	.2	-32	8	20070616b
K11A	42.77	-116.03	SKS	1.8	.2	-77	6	20070906a
K11A	42.77	-116.03	SKS	2.6	.1	-36	4	20070402a
K11A	42.77	-116.03	SKS	1.3	.2	-76	5	20070516a
K11A	42.77	-116.03	SKS	1.5	.2	-88	5	20070718a
K11A	42.77	-116.03	SKS	1.5	.3	-75	7	20070517a
K11A	42.77	-116.03	SKS	1.6	.2	-70	8	20070404c
K11A	42.77	-116.03	SKS	1.7	.3	-75	9	20070403a
K11A	42.77	-116.03	SKS	1.8	.2	-70	5	20070717a
K11A	42.77	-116.03	SKS	1.9	.2	80	7	20070325a
K12A	42.63	-114.90	SKS	1.3	.2	-78	9	20070517a
L02A	42.15	-123.60	SKS	1.2	.2	9	7	20070421a
L02A	42.15	-123.60	SKS	1.6	.1	71	8	20070726a
L04A	42.17	-121.89	SKS	1.5	.2	33	10	20070731c
L04A	42.17	-121.89	SKS	2.4	.1	53	4	20070421a
L05A	42.04	-120.83	SKS	1.2	.1	56	10	20070820a
L05A	42.04	-120.83	SKS	1.4	0	64	2	20070726a

L05A	42.04	-120.83	SKS	1.8	.1	80	6	20070906a
L07A	42.01	-119.34	SKS	.9	.1	-77	6	20070404c
L07A	42.01	-119.34	SKS	1.5	.2	88	6	20070516a
L07A	42.01	-119.34	SKS	1.7	.2	-66	6	20070718a
L07A	42.01	-119.34	SKS	2.0	.1	67	3	20060917a
L07A	42.01	-119.34	SKS	2.1	.3	77	5	20060916a
L07A	42.01	-119.34	SKS	3.2	.2	-82	2	20060624a
L07A	42.01	-119.34	SKS	1.0	.2	-40	4	20070927a
L07A	42.01	-119.34	SKS	1.5	.2	70	8	20070726a
L07A	42.01	-119.34	SKS	1.9	.2	84	9	20070718a
L07A	42.01	-119.34	SKS	2.3	.1	-85	4	20070906a
L08A	42.19	-118.34	SKS	1.9	.1	86	7	20070517a
L08A	42.19	-118.34	SKS	2.1	.1	82	7	20070906a
L08A	42.19	-118.34	SKS	2.4	.2	-72	4	20070131a
L08A	42.19	-118.34	SKS	2.6	.2	63	8	20070420a
L08A	42.19	-118.34	SKS	.8	.1	-68	5	20060807a
L08A	42.19	-118.34	SKS	.8	.1	-69	5	20060807a
L08A	42.19	-118.34	SKS	1.0	.2	87	5	20060917a
L08A	42.19	-118.34	SKS	1.1	.1	-69	9	20070403a
L08A	42.19	-118.34	SKS	2.0	.2	-88	3	20070325a
L08A	42.19	-118.34	SKS	2.1	.3	81	7	20070516a
L08A	42.19	-118.34	SKS	2.2	.3	-86	4	20070517a
L08A	42.19	-118.34	SKS	2.4	.2	-82	4	20061009a
L08A	42.19	-118.34	SKS	2.4	.3	-73	5	20070131a
L08A	42.19	-118.34	SKS	2.7	.3	88	5	20070529b

DOI: 10.1038/NGEO526

L09A	42.01	-117.67	SKS	1.5	.2	-81	10	20070517a
L09A	42.01	-117.67	SKS	1.5	.1	-59	8	20070928b
L09A	42.01	-117.67	SKS	2.1	.1	-86	7	20070906a
L09A	42.01	-117.66	SKS	.8	.1	-60	5	20060807a
L09A	42.01	-117.66	SKS	.9	.2	-89	5	20060917a
L09A	42.01	-117.66	SKS	2.5	.2	70	6	20070325a
L10A	42.07	-116.47	SKS	1.2	.2	-39	9	20070927a
L10A	42.07	-116.47	SKS	1.9	.2	-76	6	20070906a
L10A	42.07	-116.47	SKS	2.1	.2	-76	8	20070718a
L10A	42.07	-116.47	SKS	2.2	.2	78	8	20070420a
L10A	42.07	-116.47	SKS	.5	.1	-51	8	20070614a
L10A	42.07	-116.47	SKS	1.3	.3	87	5	20070517a
L10A	42.07	-116.47	SKS	1.4	.3	-83	6	20070602a
L10A	42.07	-116.47	SKS	1.6	.2	-83	3	20070516a
L10A	42.07	-116.47	SKS	2.3	.3	-72	7	20070718a
L11A	42.16	-115.75	SKS	.2	.2	-46	6	20070614a
L11A	42.16	-115.75	SKS	.5	0	-54	4	20070529b
L11A	42.16	-115.75	SKS	.8	.2	-50	9	20070628a
L11A	42.16	-115.75	SKS	.9	.2	-67	7	20070403a
L11A	42.16	-115.75	SKS	1.3	.2	-70	9	20070404c
L11A	42.16	-115.75	SKS	1.9	.3	-76	5	20070517a
L11A	42.16	-115.75	SKS	1.3	.1	-45	6	20070927a
L11A	42.16	-115.75	SKS	1.4	.1	-68	9	20070727a
L11A	42.16	-115.75	SKS	1.6	.1	-89	6	20070404c
L11A	42.16	-115.75	SKS	2.4	.1	-69	2	20070906a

L12A	42.14	-115.01	SKS	1.4	.3	-81	9	20070516a
L12A	42.14	-115.02	SKS	1.1	.1	-42	5	20070927a
L12A	42.14	-115.02	SKS	1.8	.2	77	8	20070420a
L12A	42.14	-115.02	SKS	2.9	.2	-59	4	20070906a
L13A	42.08	-113.94	SKS	.7	.1	-65	6	20070404c
LRL	35.48	-117.68	SKS	1.6	.2	-59	7	20050516a
LRL	35.48	-117.68	SKS	2.2	.2	-47	3	20051015a
M01C	41.84	-124.12	SKS	2.0	.2	47	6	20070816a
M02C	41.39	-122.85	SKS	1.5	.2	32	10	20070926a
M02C	41.39	-122.85	SKS	1.7	.2	86	6	20070726a
M04C	41.78	-121.84	SKS	1.6	.2	61	10	20070726a
M05C	41.35	-121.15	SKS	1.1	.1	67	10	20070726a
M05C	41.35	-121.15	SKS	1.4	.2	40	10	20070421a
M06C	41.20	-120.48	SKS	1.4	0	63	4	20070726a
M06C	41.20	-120.48	SKS	2.3	.2	58	4	20070906a
M07A	41.38	-119.17	SKS	1.7	.1	-53	9	20070404c
M07A	41.38	-119.17	SKS	1.9	.1	78	4	20070517a
M07A	41.38	-119.17	SKS	2.2	.2	-79	7	20070820a
M07A	41.38	-119.17	SKS	2.4	.2	-84	6	20070529b
M07A	41.38	-119.17	SKS	2.4	.1	79	6	20070906a
M07A	41.38	-119.17	SKS	1.6	.3	83	5	20060916a
M07A	41.38	-119.17	SKS	1.9	.2	87	8	20070517a
M08A	41.44	-118.38	SKS	1.3	.1	-77	8	20070927a
M08A	41.44	-118.38	SKS	1.8	.2	-84	8	20070404c
M08A	41.44	-118.38	SKS	2.0	.1	77	6	20070727a

DOI: 10.1038/NGEO526

M08A	41.44	-118.38	SKS	2.0	.2	79	7	20070517a
M08A	41.44	-118.38	SKS	2.2	.2	79	6	20070820a
M08A	41.44	-118.38	SKS	2.4	0	90	3	20070906a
M08A	41.44	-118.37	SKS	.9	.2	-72	6	20060807a
M08A	41.44	-118.37	SKS	1.8	.1	-78	7	20070718a
M08A	41.44	-118.37	SKS	1.9	.2	-67	7	20070403a
M08A	41.44	-118.37	SKS	2.7	.1	-88	3	20060916a
M09A	41.42	-117.45	SKS	.8	.1	-65	6	20060807a
M09A	41.42	-117.45	SKS	1.8	.1	88	10	20070906a
M09A	41.42	-117.45	SKS	1.9	.3	-73	9	20060811a
M09A	41.42	-117.45	SKS	2.0	.2	-73	8	20070517a
M09A	41.42	-117.45	SKS	2.0	.2	-88	4	20070928b
M09A	41.42	-117.45	SKS	2.6	.2	66	8	20060903a
M10A	41.52	-116.54	SKS	.6	.2	-50	5	20070529a
M10A	41.52	-116.54	SKS	.9	.3	61	9	20060916a
M10A	41.52	-116.54	SKS	1.0	.2	-56	5	20061003a
M10A	41.52	-116.54	SKS	1.1	.1	-69	4	20060807a
M10A	41.52	-116.54	SKS	1.3	.2	-74	9	20070404a
M10A	41.52	-116.54	SKS	1.3	.3	-81	7	20070718a
M10A	41.52	-116.54	SKS	1.5	.2	-87	9	20070727a
M10A	41.52	-116.54	SKS	1.6	.2	88	6	20070928b
M10A	41.52	-116.54	SKS	1.7	.2	-74	5	20070517a
M10A	41.52	-116.54	SKS	1.9	.2	-76	6	20070906a
M11A	41.43	-115.79	SKS	1.4	.1	81	8	20070906a
M11A	41.43	-115.79	SKS	1.6	.2	61	6	20070727a

M11A	41.43	-115.79	SKS	.6	.1	-76	6	20060807a
M11A	41.43	-115.79	SKS	.8	.3	-76	7	20070403a
M11A	41.43	-115.79	SKS	.9	.2	-83	8	20070404a
M11A	41.43	-115.79	SKS	1.4	.2	83	6	20060903a
M12A	41.41	-114.91	SKS	.5	.2	75	6	20070325a
M12A	41.41	-114.91	SKS	.6	.1	-58	7	20060807a
M12A	41.41	-114.91	SKS	.6	.2	-43	7	20060815a
M12A	41.41	-114.91	SKS	.7	.1	-72	6	20060516a
M12A	41.41	-114.91	SKS	1.0	.2	-58	7	20070403a
M12A	41.41	-114.91	SKS	1.0	.2	-64	7	20061003a
M13A	41.36	-114.16	SKS	.5	.2	-63	8	20070404a
M13A	41.36	-114.16	SKS	.6	.1	-64	5	20070404a
M13A	41.36	-114.16	SKS	.7	.1	-60	4	20060807a
M13A	41.36	-114.16	SKS	.7	.2	-46	6	20070529a
M13A	41.36	-114.16	SKS	.8	.3	-43	8	20061017a
MDW	38.89	-112.36	SKS	1.0	.2	-19	12	19950625b
MNV	38.43	-118.15	SKS	.4	.1	44	9	20050604a
MNV	38.43	-118.15	SKS	.4	.2	-87	6	20030821a
MNV	38.43	-118.15	SKS	.5	.2	-39	9	20060530a
MNV	38.43	-118.15	SKS	.5	.2	35	7	19990826a
MNV	38.43	-118.15	SKS	.6	.2	-78	7	20000815a
MNV	38.43	-118.15	SKS	.7	.1	51	6	20010605a
MNV	38.43	-118.15	SKS	.9	.2	86	9	20011218a
MNV	38.43	-118.15	SKS	.9	.3	37	9	20030311a
MNV	38.43	-118.15	SKS	1.0	.2	-67	7	20030930b

DOI: 10.1038/NGEO526

MNV	38.43	-118.15	SKS	1.1	.2	87	6	20040722a
MNV	38.43	-118.15	SKS	1.6	.2	-66	5	19950625a
MNV	38.43	-118.15	SKS	1.7	.3	-80	9	20051015a
MNV	38.43	-118.15	SKS	2.0	.1	-71	5	20030711a
MPM	36.05	-117.49	SKS	2.1	.2	-66	4	20051121a
N06A	40.74	-119.83	SKS	1.4	.1	66	8	20070726a
N06A	40.74	-119.83	SKS	1.5	.2	61	10	20070117a
N06A	40.74	-119.83	SKS	1.7	.2	51	8	20070820a
N06A	40.74	-119.83	SKS	1.9	.1	73	4	20070906a
N06A	40.74	-119.83	SKS	.7	.2	-84	7	20060903a
N06A	40.74	-119.83	SKS	.8	.2	44	8	20070722a
N06A	40.74	-119.83	SKS	.8	.3	43	9	20070722a
N06A	40.74	-119.83	SKS	1.0	.2	-85	8	20070516a
N06A	40.74	-119.83	SKS	1.4	.2	69	6	20070121a
N06A	40.74	-119.83	SKS	1.6	.1	62	7	20070325a
N06A	40.74	-119.83	SKS	1.6	.3	71	9	20060916a
N07B	40.77	-118.97	SKS	.7	.1	49	7	20060916a
N07B	40.77	-118.97	SKS	.9	.2	-75	7	20070404a
N07B	40.77	-118.97	SKS	1.1	.2	63	8	20070121a
N07B	40.78	-118.97	SKS	2.3	.1	-87	4	20070906a
N08A	40.78	-118.13	SKS	1.9	.1	-73	4	20070906a
N08A	40.78	-118.13	SKS	.2	.1	-54	3	20070529a
N08A	40.78	-118.13	SKS	.4	.1	-52	5	20060815a
N08A	40.78	-118.13	SKS	.8	.3	-66	7	20070404a
N08A	40.78	-118.13	SKS	1.0	.2	-67	6	20061003a

N08A	40.78	-118.13	SKS	1.0	.2	-85	8	20070517a
N08A	40.78	-118.13	SKS	1.1	.3	-79	6	20070602a
N08A	40.78	-118.13	SKS	1.1	.3	-82	6	20070516a
N08A	40.78	-118.13	SKS	1.2	.1	-68	4	20070718a
N09A	40.85	-117.52	SKS	1.8	.1	-85	6	20070906a
N09A	40.85	-117.52	SKS	.6	.2	-65	7	20060807a
N09A	40.85	-117.52	SKS	.6	.2	-65	7	20060807a
N09A	40.85	-117.52	SKS	.9	.1	-70	5	20070404a
N09A	40.85	-117.52	SKS	.9	.1	-78	5	20060516a
N09A	40.85	-117.52	SKS	.9	.2	-80	6	20060516a
N09A	40.85	-117.52	SKS	.9	.2	59	8	20060916a
N09A	40.85	-117.52	SKS	1.4	.3	-77	8	20070516a
N09A	40.85	-117.52	SKS	1.8	.2	86	5	20061009a
N09A	40.85	-117.52	SKS	1.8	.2	86	5	20061009a
N10A	40.71	-116.50	SKS	.6	.2	54	7	20070722a
N10A	40.71	-116.50	SKS	.9	.2	-63	8	20061003a
N10A	40.71	-116.50	SKS	.9	.2	-65	9	20070404a
N11A	40.81	-115.73	SKS	.2	.2	9	9	20060917a
N11A	40.81	-115.73	SKS	.4	.2	-63	7	20060807a
N11A	40.81	-115.73	SKS	.6	.2	-56	3	20061003a
N11A	40.81	-115.73	SKS	.7	.2	56	7	20070722a
N11A	40.81	-115.73	SKS	.8	.2	-62	9	20070404a
N11A	40.81	-115.73	SKS	.8	.2	79	6	20061009a
N11A	40.81	-115.73	SKS	.8	.3	-79	7	20070131a
N11A	40.81	-115.73	SKS	1.5	.2	-65	7	20060903a

DOI: 10.1038/NGEO526

N12A	40.85	-115.04	SKS	.9	.1	-89	10	20070906a
N12A	40.85	-115.04	SKS	1.9	.2	-84	2	20070816a
N12A	40.85	-115.03	SKS	.5	.1	-43	6	20070529a
N12A	40.85	-115.03	SKS	.5	.2	-42	9	20070628a
N12A	40.85	-115.03	SKS	.6	.3	-55	8	20070404a
N12A	40.85	-115.03	SKS	1.0	.1	-57	6	20061003a
N12A	40.85	-115.03	SKS	1.0	.2	-54	6	20070403a
N12A	40.85	-115.03	SKS	1.2	.3	-83	7	20070420b
N13A	40.85	-114.20	SKS	.5	.2	-37	5	20070722a
N13A	40.85	-114.20	SKS	.7	.2	-63	6	20061003a
N13A	40.85	-114.20	SKS	.8	.1	-59	4	20060807a
N13A	40.85	-114.20	SKS	1.0	.2	-31	6	20060916a
N14A	40.85	-113.18	SKS	.6	.2	-61	7	20070404a
N14A	40.85	-113.18	SKS	.7	.2	-39	9	20070614a
N14A	40.85	-113.18	SKS	.9	.2	-43	7	20070529a
N14A	40.85	-113.18	SKS	1.0	.4	-44	8	20070628a
N15A	40.89	-112.52	SKS	.5	.2	-45	8	20070614a
N15A	40.89	-112.52	SKS	.6	.3	-38	7	20070722a
NEE	34.82	-114.60	SKS	1.1	.1	89	6	19950823a
NEE	34.82	-114.60	SKS	1.3	.2	63	12	20000226a
NV31	38.43	-118.15	SKS	1.0	.2	61	7	20050116a
NV31	38.43	-118.15	SKS	1.0	.2	61	8	20050116a
NV31	38.43	-118.15	SKS	1.1	.1	-79	5	20030930b
NV31	38.43	-118.15	SKS	1.1	.1	-82	5	20030930b
NV31	38.43	-118.15	SKS	1.2	.2	89	7	20040722a

NV31	38.43	-118.15	SKS	1.2	.2	89	7	20040722a
NV31	38.43	-118.15	SKS	1.4	.2	88	6	20041015a
NV31	38.43	-118.15	SKS	1.4	.2	88	6	20041015a
NV31	38.43	-118.15	SKS	1.5	.2	-77	8	20050906a
NV31	38.43	-118.15	SKS	1.5	.2	-77	8	20050906a
NV31	38.43	-118.15	SKS	1.8	.2	-40	8	20060526a
NV31	38.43	-118.15	SKS	1.8	.4	-81	9	20051015a
NV31	38.43	-118.15	SKS	2.2	.3	-67	5	20051121a
NV31	38.43	-118.15	SKS	2.2	.3	-67	5	20051121a
NV32	38.33	-118.29	SKS	.1	.1	60	8	20030814a
NV32	38.33	-118.29	SKS	.8	0	73	5	20030930b
NV32	38.33	-118.29	SKS	.8	.1	67	8	20030930b
NV32	38.33	-118.29	SKS	1.0	.2	-71	8	20041015a
NV32	38.33	-118.29	SKS	1.4	0	-79	4	20050205c
NV32	38.33	-118.29	SKS	1.4	0	-79	4	20050205c
NV33	38.48	-118.41	SKS	.4	.1	-87	5	20040810a
NV33	38.48	-118.41	SKS	.5	0	14	6	20040207a
NV33	38.48	-118.41	SKS	.5	.2	20	9	20040528a
NV33	38.48	-118.41	SKS	.6	.1	-2	6	20040513a
NV33	38.48	-118.41	SKS	.7	.1	14	9	20040728a
NV33	38.48	-118.41	SKS	.7	.2	-14	8	20041008a
NV33	38.48	-118.41	SKS	.8	.1	16	6	20041126a
O04C	40.32	-121.09	SKS	1.4	.1	48	8	20070726a
O04C	40.32	-121.09	SKS	1.6	.2	76	8	20070820a
O04C	40.32	-121.09	SKS	2.3	.2	42	8	20070317a

DOI: 10.1038/NGEO526

O06A	40.16	-119.82	SKS	.3	.2	44	7	20070529a
O06A	40.16	-119.82	SKS	.4	.2	51	9	20070529a
O06A	40.16	-119.82	SKS	.5	.2	51	9	20070722a
O06A	40.16	-119.82	SKS	1.0	.1	10	7	20060917a
O07A	40.16	-118.87	SKS	.3	.1	6	6	20060917a
O07A	40.16	-118.87	SKS	.4	.1	44	8	20060528a
O07A	40.16	-118.87	SKS	.5	.2	59	9	20060916a
O07A	40.16	-118.87	SKS	.5	.2	60	9	20070121a
O08A	40.29	-118.15	SKS	.3	.2	-62	9	20070529a
O08A	40.29	-118.15	SKS	.5	.3	-10	6	20060917a
O08A	40.29	-118.15	SKS	.6	.2	-84	8	20070404a
O08A	40.29	-118.15	SKS	.8	.4	88	9	20070517a
O08A	40.29	-118.15	SKS	1.3	.3	86	9	20070602a
O09A	40.16	-117.19	SKS	.5	.2	54	9	20070722a
O09A	40.16	-117.19	SKS	1.0	.2	-64	6	20061003a
O09A	40.16	-117.19	SKS	1.3	.3	-74	7	20070718a
O09A	40.16	-117.19	SKS	1.4	.2	-58	7	20070403a
O10A	40.29	-116.50	SKS	.3	.2	-54	7	20061003a
O10A	40.29	-116.50	SKS	.4	.2	47	9	20070614a
O10A	40.29	-116.50	SKS	.4	.2	54	9	20070722a
O10A	40.29	-116.50	SKS	.8	.2	-76	5	20070517a
O10A	40.29	-116.50	SKS	.8	.3	-76	6	20070516a
O10A	40.29	-116.50	SKS	.9	.3	-76	9	20060903a
O10A	40.29	-116.50	SKS	1.0	.2	-77	9	20060903a
O11A	40.13	-115.65	SKS	.5	.1	-70	8	20070404a

O12A	40.26	-114.74	SKS	.4	.1	-52	8	20070529a
O12A	40.26	-114.74	SKS	.4	.2	-83	9	20070517a
O12A	40.26	-114.74	SKS	.5	.1	-66	6	20060807a
O12A	40.26	-114.74	SKS	.5	.1	-79	7	20060602a
O12A	40.26	-114.74	SKS	.6	.2	-71	9	20061003a
O12A	40.26	-114.74	SKS	.8	.2	-39	9	20070722a
O13A	40.13	-113.98	SKS	.6	.2	-43	4	20070722a
O13A	40.13	-113.98	SKS	.8	.1	-51	9	20070628a
O13A	40.13	-113.98	SKS	.9	.2	-44	8	20070614a
P06A	39.67	-119.89	SKS	.7	.2	57	6	20070722a
P08A	39.69	-118.08	SKS	.7	.2	-82	5	20060516a
P09A	39.55	-117.14	SKS	.5	.2	51	8	20070722a
P10A	39.62	-116.46	SKS	2.2	.2	-72	6	20070420b
P10A	39.62	-116.46	SKS	.3	.2	44	9	20061017a
P10A	39.62	-116.46	SKS	.6	.2	56	8	20070722a
P10A	39.62	-116.46	SKS	.6	.3	53	9	20060916a
P11A	39.55	-115.75	SKS	.6	.2	-51	6	20061017a
P11A	39.55	-115.75	SKS	.6	.2	-72	5	20070403a
P12A	39.47	-114.91	SKS	.6	.2	-25	10	20070628a
P12A	39.47	-114.90	SKS	.4	.2	-82	8	20060903a
P12A	39.47	-114.90	SKS	.6	.1	-45	5	20061017a
P12A	39.47	-114.90	SKS	.6	.1	-56	7	20070628a
P12A	39.47	-114.90	SKS	.6	.2	-36	6	20070722a
P15A	39.57	-112.28	SKS	1.5	.2	-8	4	20070722b
P16A	39.60	-111.66	SKS	.8	.1	-45	14	20070722a

DOI: 10.1038/NGEO526

Q07A	38.93	-118.80	SKS	.6	.2	43	8	20070628a
Q07A	38.93	-118.80	SKS	.7	.2	43	8	20070529a
Q07A	38.93	-118.80	SKS	.7	.2	69	7	20070121a
Q08A	38.86	-117.93	SKS	.5	.2	39	9	20060815a
Q08A	38.86	-117.93	SKS	.5	.2	40	7	20061017a
Q08A	38.86	-117.93	SKS	.5	.2	82	6	20061009a
Q08A	38.86	-117.93	SKS	.8	.3	-29	7	20070529a
Q08A	38.86	-117.93	SKS	.9	.1	39	6	20060528a
Q08A	38.86	-117.93	SKS	.9	.3	44	9	20070421a
Q08A	38.86	-117.93	SKS	1.0	.1	38	9	20070529a
Q08A	38.86	-117.93	SKS	.8	.1	69	4	20060516a
Q09A	38.83	-117.18	SKS	.2	.2	44	8	20061017a
Q09A	38.83	-117.18	SKS	.3	.2	36	8	20070529a
Q10A	38.82	-116.40	SKS	.4	.2	14	8	20070517a
Q10A	38.82	-116.40	SKS	.8	.3	39	9	20070616a
Q11A	38.84	-115.65	SKS	.2	0	41	8	20070529a
Q11A	38.84	-115.65	SKS	.3	.2	47	9	20061017a
Q11A	38.84	-115.65	SKS	.3	.2	53	7	20070421a
Q12A	39.04	-114.83	SKS	.4	.2	-39	9	20070722a
R08A	38.34	-118.10	SKS	.4	.2	37	6	20061017a
R08A	38.34	-118.10	SKS	.5	.2	56	8	20070121a
R08A	38.34	-118.10	SKS	.7	.3	-80	6	20070517a
R09A	38.23	-117.07	SKS	.3	.1	49	9	20061107a
R09A	38.23	-117.07	SKS	.3	.2	63	9	20070529a
R09A	38.23	-117.07	SKS	.4	.2	-85	9	20070517a

R09A	38.23	-117.07	SKS	.7	.3	58	8	20070722a
R12A	38.32	-114.60	SKS	.3	.1	43	6	20070628a
R12A	38.32	-114.60	SKS	.5	.1	23	8	20070403a
R17A	38.41	-110.71	SKS	.9	.2	8	8	20070927a
R17A	38.41	-110.71	SKS	1.6	.2	9	6	20070727a
S08C	37.49	-118.17	SKS	1.3	.3	67	9	20070121a
S08C	37.49	-118.17	SKS	1.5	.2	66	9	20060916a
S08C	37.49	-118.17	SKS	1.8	.2	86	5	20051121a
S08C	37.49	-118.17	SKS	2.7	.1	74	3	20070529a
S09A	37.72	-117.22	SKS	.3	.1	40	8	20070614a
S09A	37.72	-117.22	SKS	.6	.2	62	9	20060916a
S09A	37.72	-117.22	SKS	.8	.3	62	9	20070117a
S10A	37.92	-116.59	SKS	.3	.2	-56	6	20070628a
S10A	37.92	-116.59	SKS	.4	.1	-58	5	20070614a
S10A	37.92	-116.59	SKS	.4	.2	-85	7	20070517a
S11A	37.64	-115.74	SKS	.4	.2	70	8	20070722a
S13A	37.58	-113.86	SKS	.7	.1	67	12	20070913c
S13A	37.58	-113.86	SKS	1.2	.2	55	11	20070504a
S13A	37.58	-113.86	SKS	1.3	.2	62	4	20070816a
S14A	37.76	-113.16	SKS	.4	.1	59	7	20070529a
S17A	37.63	-110.80	SKS	1.5	.2	74	2	20070816a
SLA	35.89	-117.28	SKS	.9	.2	-86	11	19990420a
SLA	35.89	-117.28	SKS	1.3	.1	88	6	20060516a
SLA	35.89	-117.28	SKS	1.5	.2	-70	14	20040307a
T11A	37.24	-115.22	SKS	.5	.2	-85	8	20070517a

DOI: 10.1038/NGEO526

T12A	36.72	-114.71	SKS	.2	.1	44	7	20070529a
T14A	37.06	-113.08	SKS	.5	.2	51	7	20070529a
T14A	37.06	-113.08	SKS	1.4	.3	20	9	20070403a
T14A	37.06	-113.08	SKS	.8	.1	39	13	20070402b
T15A	37.01	-112.38	SKS	1.2	.2	64	4	20070816a
T16A	36.98	-111.51	SKS	.9	.1	70	5	20070816a
TAKO	43.74	-124.08	SKS	1.2	.1	67	9	20070726a
TPH	38.07	-117.22	SKS	.7	.2	79	10	20050205c
TPH	38.07	-117.22	SKS	.7	.2	70	11	20011012a
TPH	38.07	-117.22	SKS	.8	0	83	8	19970525a
TPH	38.07	-117.22	SKS	.8	.2	-86	14	19970904a
TPH	38.07	-117.22	SKS	1.3	.2	-73	7	20040722a
TPH	38.07	-117.22	SKS	1.4	.2	-57	5	20030930b
TPH	38.07	-117.22	SKS	1.4	.2	53	11	20070930d
TPH	38.07	-117.22	SKS	.4	.1	40	5	20020228a
TPH	38.07	-117.22	SKS	.4	.1	54	7	20021017a
TPH	38.07	-117.22	SKS	.4	.1	59	6	20040207a
TPH	38.07	-117.22	SKS	.4	.1	61	6	20040728a
TPH	38.07	-117.22	SKS	.4	.2	40	9	20020228a
TPH	38.07	-117.22	SKS	.5	.1	47	8	20040513a
TPH	38.07	-117.22	SKS	.5	.2	17	9	20061017a
TPH	38.07	-117.22	SKS	.5	.3	61	8	20010911a
TPH	38.07	-117.22	SKS	.6	.1	46	9	20030725a
TPH	38.07	-117.22	SKS	.6	.1	70	5	20050205a
TPH	38.07	-117.22	SKS	.6	.1	80	7	20041015a

TPH	38.07	-117.22	SKS	.6	.1	83	6	19990920a
TPH	38.07	-117.22	SKS	.6	.1	84	5	19990920a
TPH	38.07	-117.22	SKS	.6	.1	88	7	19970503a
TPH	38.07	-117.22	SKS	.6	.2	-79	5	20030930a
TPH	38.07	-117.22	SKS	.6	.2	19	9	20070529a
TPH	38.07	-117.22	SKS	.6	.2	70	8	20010614a
TPH	38.07	-117.22	SKS	.6	.2	71	8	20050205a
TPH	38.07	-117.22	SKS	.6	.2	79	9	19991211a
TPH	38.07	-117.22	SKS	.6	.2	81	7	20010817a
TPH	38.07	-117.22	SKS	.6	.2	82	6	20010817a
TPH	38.07	-117.22	SKS	.6	.2	82	7	20041015a
TPH	38.07	-117.22	SKS	.6	.3	0	9	20061107a
TPH	38.07	-117.22	SKS	.7	.1	-87	4	20030930a
TPH	38.07	-117.22	SKS	.7	.1	62	8	20011012a
TPH	38.07	-117.22	SKS	.7	.1	79	9	19991211a
TPH	38.07	-117.22	SKS	.8	.1	-83	5	20030504a
TPH	38.07	-117.22	SKS	.8	.1	79	6	19970503a
TPH	38.07	-117.22	SKS	.8	.1	88	5	19970525a
TPH	38.07	-117.22	SKS	.8	.1	89	6	19970525a
TPH	38.07	-117.22	SKS	.8	.2	-75	7	20000614a
TPH	38.07	-117.22	SKS	.8	.2	-75	7	20000614a
TPH	38.07	-117.22	SKS	.8	.2	-86	7	20050723a
TPH	38.07	-117.22	SKS	.8	.2	79	9	20040722a
TPH	38.07	-117.22	SKS	.9	.1	-83	8	20000815a
TPH	38.07	-117.22	SKS	.9	.1	-83	6	20050516a

DOI: 10.1038/NGEO526

TPH	38.07	-117.22	SKS	.9	.1	-84	4	20000815a
TPH	38.07	-117.22	SKS	.9	.1	87	5	19970904a
TPH	38.07	-117.22	SKS	1.0	.2	88	6	20040519a
TPNV	36.94	-116.24	SKS	.7	0	65	6	19950823a
TPNV	36.94	-116.24	SKS	.7	.1	68	7	19950823a
TUQ	35.43	-115.92	SKS	1.0	.2	-89	10	20070928b
TUQ	35.43	-115.92	SKS	1.6	.1	-85	6	20040602a
TUQ	35.43	-115.92	SKS	1.6	.2	79	9	20050117a
U10A	36.41	-116.33	SKS	.3	.1	39	8	20061017a
U10A	36.41	-116.33	SKS	.5	.2	47	9	20070722a
U10A	36.41	-116.33	SKS	.6	.2	20	9	20070404a
U11A	36.42	-115.38	SKS	.5	.1	46	8	20061017a
U12A	36.43	-114.54	SKS	.7	.1	40	10	20070628a
U12A	36.43	-114.54	SKS	1.0	.2	48	6	20071013a
U12A	36.43	-114.54	SKS	1.4	.2	41	14	20070403a
U12A	36.43	-114.53	SKS	.7	.2	47	8	20061107a
U12A	36.43	-114.53	SKS	.7	.2	48	8	20061017a
U12A	36.43	-114.53	SKS	1.0	.2	56	8	20060815a
U12A	36.43	-114.53	SKS	1.6	.4	77	8	20070529a
U14A	36.41	-113.18	SKS	.8	.1	46	10	20070402b
U14A	36.41	-113.18	SKS	1.6	.2	63	5	20070816a
U14A	36.41	-113.18	SKS	1.7	.1	44	8	20070715a
U17A	36.60	-110.66	SKS	1.1	.2	66	6	20070816a
UT54	37.41	-110.51	SKS	.8	.2	45	14	20000717a
UT54	37.41	-110.51	SKS	1.7	.2	53	4	20010109a

V11A	35.83	-115.43	SKS	.2	.2	-83	6	20070517a
V11A	35.83	-115.43	SKS	.5	.2	49	7	20070722a
V11A	35.83	-115.43	SKS	.7	.2	50	9	20070722a
V12A	35.72	-114.85	SKS	.4	.2	37	8	20061107a
V12A	35.72	-114.85	SKS	.5	.1	38	7	20070529a
V12A	35.72	-114.85	SKS	.6	.1	-81	6	20060903a
V12A	35.72	-114.85	SKS	1.9	.1	37	7	20070501a
V13A	35.85	-113.98	SKS	1.1	.1	56	4	20070816a
V13A	35.85	-113.98	SKS	1.9	.2	23	8	20070731c
V14A	35.63	-113.11	SKS	1.3	.1	51	4	20070816a
V15A	35.81	-112.17	SKS	1.0	.2	26	14	20070928b
VTV	34.56	-117.33	SKS	1.1	.2	66	12	20020814a
VTV	34.56	-117.33	SKS	1.7	.1	-81	5	20051015a
W13A	35.09	-113.89	SKS	.9	.1	51	12	20070723a
W13A	35.09	-113.89	SKS	1.0	.1	32	6	20070628a
W13A	35.09	-113.89	SKS	1.1	.1	62	6	20070816a
W13A	35.09	-113.89	SKS	2.0	.2	25	6	20070731c
W14A	35.21	-113.08	SKS	1.0	.1	52	4	20070816a
W15A	35.17	-112.27	SKS	.8	.2	25	14	20070402b
W15A	35.17	-112.27	SKS	1.3	0	37	5	20070816a
W15A	35.17	-112.27	SKS	1.6	.2	44	8	20070618a
W15A	35.17	-112.27	SKS	1.7	.2	32	6	20070723a
WHA00	35.87	-117.73	SKS	1.1	.2	-73	10	19990420a
WHAS5	35.85	-117.74	SKS	1.1	.2	-75	7	19990420a
WUAZ	35.51	-111.37	SKS	1.2	.2	29	13	20030912a

DOI: 10.1038/NGEO526

WUAZ	35.51	-111.37	SKS	1.3	.2	56	6	20020924b
WUAZ	35.51	-111.37	SKS	1.4	.1	65	4	20070816a
WUAZ	35.51	-111.37	SKS	1.7	.2	30	10	20070805a
WUAZ	35.51	-111.37	SKS	2.2	.1	19	2	20020917a
WVOR	42.43	-118.64	SKS	1.7	.2	72	8	20070726a
WVOR	42.43	-118.64	SKS	2.3	.1	-89	6	20070906a
WVOR	42.43	-118.64	SKS	2.8	.2	81	5	20070131a
YBH	41.73	-122.71	SKS	1.1	.1	78	8	20070726a
YBH	41.73	-122.71	SKS	1.4	.2	20	8	20070731c

Supplementary Table 2: List of events for shear wave splitting measurements.

Event ID, events used for measurements in Supplementary Table 1; GMT, Greenwich Mean Time.

Event_ID	Time(GMT)	Latitude(∫N)	Longitude(∫E)	Depth(km)	Magnitude(mb)
19950117a	16:54:12	-20.87	-179.22	637	6.0
19950505a	03:53:47	12.62	125.31	33	6.2
19950625a	02:10:41	-3.28	150.36	45	6.3
19950625b	06:59:05	24.60	121.71	47	5.8
19950629a	12:24:03	-19.46	169.24	144	6.2
19950703a	19:50:50	-29.20	-177.61	33	6.5
19950823a	07:06:02	18.86	145.19	596	6.3
19960827a	06:24:07	-22.57	-179.79	575	6.0
19961105a	09:41:34	-31.16	180.00	369	5.9
19970503a	16:46:02	-31.79	-179.38	108	6.6
19970525a	23:22:33	-32.12	179.79	333	6.2
19970813a	04:45:04	25.03	125.77	55	6.0
19970904a	04:23:37	-26.57	178.34	625	6.3
19990420a	19:04:08	-31.89	-179.04	96	6.2
19990719a	02:17:03	-28.63	-177.61	39	6.3
19990801a	08:39:04	-30.37	-177.83	10	6.4
19990826a	01:24:42	10.38	126.01	63	6.1
19990913a	11:55:28	40.71	30.05	13	5.8
19990920a	17.47.18	23.77	120.98	33	6.2
19991101a	17:53:00	23.38	121.52	33	6.1

DOI: 10.1038/NGEO526

19991126a	02:56:07	-30.23	-177.68	33	5.9
19991211a	07:18:41	-13.91	167.19	203	5.8
20000226a	08:11:48	13.80	144.78	132	6.0
20000610a	09:17:53	-11.45	166.24	33	5.9
20000614a	02:15:25	-25.52	178.05	605	5.9
20000621a	16:25:06	14.11	144.96	112	6.0
20000717a	22:53:47	36.28	70.92	141	6.0
20000815a	04:30:08	-31.51	179.73	358	6.0
20010109a	16:49:28	-14.93	167.17	103	6.3
20010603a	02:41:57	-29.67	-178.63	178	6.8
20010605a	15:13:58	-6.82	146.41	10	5.8
20010614a	02:35:25	24.51	122.03	32	5.9
20010817a	22:25:49	25.75	126.19	33	5.9
20010911a	14:56:50	-0.58	133.13	33	5.8
20011012a	15:02:16	12.69	144.98	37	6.7
20011218a	04:02:58	23.96	122.73	14	6.3
20020228a	01:50:48	-5.69	151.26	40	6.0
20020610a	22:48:36	10.99	140.69	33	5.9
20020630a	21:29:36	-22.20	179.25	620	6.5
20020814a	13:12:39	7.83	136.88	10	6.1
20020819a	11:01:01	-21.70	-179.51	580	6.7
20020917a	11:20:23	-3.28	142.77	10	5.9
20020924b	04:13:11	-10.54	161.20	10	6.2
20021004a	19:05:48	-20.99	-179.02	621	6.1
20021017a	04:23:55	-19.84	-178.40	628	6.4

20021210a	01:28:33	-50.03	-114.12	10	6.0
20030311a	07:27:32	-4.69	153.24	40	6.0
20030427a	16:03:40	-20.94	169.77	77	6.0
20030504a	13:15:18	-30.53	-178.23	62	6.0
20030513a	21:21:14	-17.29	167.74	33	6.0
20030711a	13:53:24	9.34	122.04	33	5.9
20030725a	09:37:45	-1.53	149.69	24	6.4
20030814a	05:14:54	39.16	20.61	10	6.2
20030821a	04:02:09	29.05	59.77	20	5.8
20030912a	06:55:55	-5.27	151.50	50	5.8
20030930a	15:22:31	-30.49	-177.18	33	6.0
20030930b	14:08:37	-30.44	-177.40	10	5.8
20040207a	02:42:35	-4.00	135.02	10	6.2
20040307a	11:08:01	-32.38	-178.19	7	5.9
20040513a	09:58:43	-3.58	150.73	10	5.8
20040519a	07:04:11	22.66	121.50	20	5.8
20040528a	12:38:44	36.25	51.62	17	6.2
20040602a	22:39:29	-30.48	-177.88	28	5.8
20040722a	09:45:14	26.49	128.89	21	6.1
20040728a	03:56:28	-0.44	133.09	13	6.0
20040810a	01:47:32	36.44	70.80	207	6.0
20041008a	08:27:53	-10.95	162.16	36	6.1
20041015a	04:08:50	24.53	122.69	94	6.4
20041126a	02:25:03	-3.61	135.40	10	6.2
20050116a	08:25:04	-25.59	-176.30	16	6.0

DOI: 10.1038/NGEO526

20050117a	10:50:32	10.99	140.68	12	5.9
20050205a	03:34:25	16.01	145.87	143	6.3
20050205c	12:23:18	5.29	123.34	525	6.4
20050210a	16:53:19	-23.10	169.22	9	6.0
20050516a	03:54:14	-32.59	-179.35	34	6.2
20050604a	14:50:48	-6.34	146.81	43	6.0
20050711a	23:06:01	-27.00	-176.32	10	6.0
20050723a	07:34:56	35.50	139.98	61	6.1
20050906a	01:16:02	24.08	122.19	32	5.8
20051015a	15:51:07	25.32	123.36	183	6.2
20051121a	15:36:30	31.02	130.00	145	5.9
20060218a	15:59:22	-5.19	152.05	44	5.9
20060226a	03:08:27	-23.61	-179.99	535	5.9
20060516a	10:39?23	-31.78	-179.31	152	6.8
20060526a	22:53:58	-7.96	110.45	13	6.0
20060528a	03:12:08	-5.72	151.13	34	5.9
20060530a	03:28:52	-3.77	140.06	30	5.9
20060602a	07:31:36	-20.84	-178.70	592	6.0
20060624a	21:15:00	-0.39	123.19	26	5.8
20060807a	22:18:54	-15.80	167.79	141	6.0
20060811a	20:54:14	2.40	96.35	22	5.8
20060815a	03:05:10	-4.67	126.73	10	6.1
20060903a	22:57:30	-24.05	178.82	568	5.9
20060916a	02:22:50	41.36	135.70	367	5.9
20060917a	09:34:14	-31.75	-67.18	142	6.2

20061003a	18:03:14	-18.87	169.00	171	5.9
20061009a	10:01:46	20.65	120.02	10	6.0
20061017a	11:25:02	-5.88	150.98	32	6.4
20061107a	13:25:36	-21.73	-68.20	121	5.8
20070117a	04:28:26	-3.32	139.83	101	6.0
20070121a	11:27:45	1.07	126.28	22	6.7
20070130a	04:54:50	-54.74	146.30	11	6.2
20070131a	03:15:52	-29.78	-178.00	34	6.1
20070317a	17:42:26	1.13	126.22	35	6.0
20070325a	00:40:01	-20.62	169.36	34	6.5
20070402a	10:49:17	-7.23	156.24	34	5.8
20070402b	12:02:23	-8.71	157.62	14	6.0
20070403a	03:35:07	36.45	70.69	222	6.2
20070403c	20:26:09	-20.63	168.99	12	6.0
20070404a	00:39:43	-7.14	156.05	10	5.9
20070404c	11:00:27	-20.71	168.83	10	5.8
20070420a	00:26:40	25.72	125.09	10	6.1
20070420b	01:45:56	25.71	125.11	9	5.9
20070421a	07:12:48	-3.55	151.27	407	5.8
20070501a	01:45:23	-7.17	155.11	10	5.8
20070504a	12:06:52	-1.41	-14.91	10	5.9
20070516a	08:56:16	20.50	100.75	24	6.4
20070517a	19:29:10	-30.66	-178.20	41	6.0
20070529a	01:03:27	-4.59	151.84	133	5.9
20070529b	09:36:05	-1.07	127.34	24	6.0

DOI: 10.1038/NGEO526

20070602a	21:34:57	23.03	101.05	5	6.3
20070614a	13:37:40	-36.21	-100.15	10	5.9
20070614b	17:41:04	-5.65	151.56	41	5.8
20070616a	01:18:47	1.15	126.41	47	5.8
20070616b	04:23:57	-7.26	155.51	10	5.8
20070618a	06:18:48	-3.57	150.95	26	6.2
20070628a	02:52:09	-7.97	154.63	10	6.3
20070715a	09:27:34	-15.38	168.60	8	6.0
20070717a	09:39:27	-26.21	-177.74	10	6.0
20070718a	00:07:35	-26.30	-177.74	10	5.8
20070722a	10:49:35	-2.80	141.66	10	5.8
20070722b	14:20:43	-2.78	141.72	10	5.8
20070723a	00:08:32	-4.47	149.85	572	5.9
20070726a	05:40:16	2.87	127.46	25	6.4
20070727a	14:46:26	-21.46	170.94	10	6.0
20070731c	22:55:31	-0.16	-17.80	11	6.2
20070805a	09:28:40	-19.15	168.72	45	6.0
20070816a	08:39:27	-9.83	159.47	10	6.1
20070820a	13:46:17	6.13	127.38	8	6.4
20070820b	21:30:45	-5.39	140.88	10	5.9
20070906a	17:51:26	24.34	122.22	53	6.1
20070913c	09:48:46	3.80	126.33	35	6.2
20070926a	12:36:26	-4.99	153.50	40	6.2
20070927a	19:57:44	-21.10	169.28	9	6.2
20070928b	01:01:48	-21.21	169.36	10	5.8

20070928f	13:38:59	22.01	142.67	276	6.7
20070930d	15:02:18	10.52	145.59	24	5.8
20071013a	17:45:53	-21.23	169.20	37	5.8